Coloration mechanisms of sol–gel NiO–TiO$_2$ layers studied by EQCM

A. Al-Kahlout, M.A. Aegerter*

[a]*Leibniz Institut für Neue Materialien INM, Im Stadtwald Geb. D2 2, Saarbruecken 66123, Germany*

Abstract

An electrochemical quartz crystal microbalance was used as a sensitive detector to analyse the mass changes occurring during the coloration/bleaching processes of sol gel NiO TiO$_2$ electrochromic layers. Double layers were deposited on gold coated quartz crystal electrode and sintered at 300 °C in air. The electrochemical process was studied in KOH electrolyte in the potential range 0.4 to + 0.57 V vs. SCE during 650 CV cycles. The current density, charge and mass were found to increase with cycling. The shape of the mass spectrum is rather complex and changes continuously by cycling. The mass of the layer increases after each cycle slowly up to about the 150th cycle then it increases strongly after about the 250th cycle. It passes through a maximum around the 570th cycle with high amplitude variation within each cycle and then decreases fast without drastic change of the cathodic charge. Finally, a complete breakdown occurs around the 650th CV cycle impeding to record any further mass variation. The study is divided in two typical regions where the mechanism of coloration is found to change by cycling. During the first 150 CV cycles, the reversible change of the mass with the charge (increase in the anodic range for $V > 0.35$ V vs. SCE and decrease in the cathodic range for $V < 0.2$ V) was related to exchange of OH$^-$ groups that involves a change of the oxidation state of Ni from 2$^+$ to 3$^+$ and vice versa leading to coloration and bleaching processes, respectively. For further cycling a model is proposed taking into account the incorporation of K(H$_2$O)$_n$$^+$ ions in the hydrated structure of the layer. The irreversible increase of both the mass and charge exchanged during each cycle is interpreted as due to an increase of the amount of Ni(OH)$_2$.

Keywords: Nio TiO$_2$ coatings; Sol gel; Electrochromism; Quartz crystal microbalance

1. Introduction

Electrochromism in oxide thin film electrodes is usually interpreted as an electron transfer reaction that accompanies the insertion of electroactive species, such as H$^+$, Li$^+$ or OH$^-$, into the amorphous or crystalline structure of the host materials, resulting in new absorption bands and consequently an altered layer coloration [1]. Understanding the mechanism of ion insertion in metal oxides during an electrochromic reaction is therefore a fundamental task to clarify the optical performance and also the eventual electrode failure. It is well known that the detailed insertion mechanisms are usually highly complex and may consist of several processes.

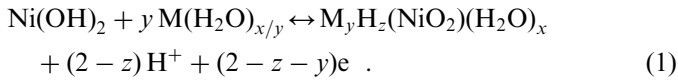Electrochromic NiO-based coatings are among the least understood material and the electrochemical mechanisms that lead to electrochromism are still controversial. It is however accepted that the coloration is due to the oxidation of Ni(II) into Ni(III) involving the transformation of Ni(OH)$_2$ into NiOOH. It is also known that there are several Ni(OH)$_2$ phases. The most popular one is called β-Ni(OH)$_2$ and can intercalate water to form the α-Ni(OH)$_2$ phase. The corresponding oxidized forms are β-NiOOH and γ-NiOOH, respectively. From the extended arguments found in the literature for explaining the electrochromism of nickel-based oxides [2–8] it can be concluded that the mechanisms of coloration/bleaching are strongly dependent on two main factors:

(i) The composition and the phase of the starting nickel oxide layer, which in turn depends on the layer deposition technique and the experimental conditions.
(ii) The kind of involved species during cycling. When a layer is tested in aqueous basic solution for instance the most probable ones are H$^+$, OH$^-$ or both but when an

aprotic Li^+ electrolyte is used, then Li^+ will be the most probable specie.
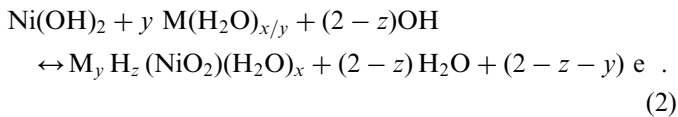
Attempts have already been made to clarify the EC mechanisms using a combination of different electrochemical and optical techniques [5,8]. Among them, the electrochemical quartz crystal microbalance (EQCM) technique has been used to address the behavior of nickel-based oxides in alkaline solution in the field of battery [9,10]. However, very few works have been reported aiming to understand the electrochromism of these materials [11,12]. This technique uses a piezoelectric quartz crystal coated with the investigated film oscillating at a defined frequency and small mass changes occurring in the layer during the electrochemical processes are detected by the shift of this frequency.

Bernard et al. [9] studied the electrochemical kinetics of the ionic exchange process of *cathodically precipitated* $Ni(OH)_2$ in 5 M alkaline solution under a sinusoidal modulation and concluded that the electrochemical reaction involves both the incorporation of hydrated cations and a deprotonation according to the reaction
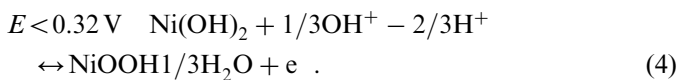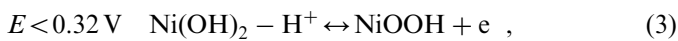
$$Ni(OH)_2 + y\,M(H_2O)_{x/y} \leftrightarrow M_y H_z(NiO_2)(H_2O)_x$$
$$+ (2-z)\,H^+ + (2-z-y)e \ . \tag{1}$$

The cations M were Li^+, Na^+, K^+, Rb^+ or Cs^+.

Based on this reaction, Cordoba-Torresi et al. [11] found that the coloration reaction of *electrochemically deposited* $Ni(OH)_2$ in a lower concentration alkaline electrolyte (1 M KOH or LiOH) involves the incorporation of hydrated cations and that the number of coordinated H_2O molecules was depending on the kind of cations according to the reaction

$$Ni(OH)_2 + y\,M(H_2O)_{x/y} + (2-z)OH$$
$$\leftrightarrow M_y\,H_z\,(NiO_2)(H_2O)_x + (2-z)\,H_2O + (2-z-y)\,e \ . \tag{2}$$

Bange et al. [12] studied the coloration mechanism of *e-beam evaporated* $Ni(OH)_x$ films in 1 M NaOH and 1 M NaOD in the potential range -0.5 to $+0.6$ V vs. SCE. They divided the coloration process (anodic range) into two main steps summarized by the following equations:

$$E < 0.32\,V \quad Ni(OH)_2 - H^+ \leftrightarrow NiOOH + e \ , \tag{3}$$

$$E < 0.32\,V \quad Ni(OH)_2 + 1/3OH^+ - 2/3H^+$$
$$\leftrightarrow NiOOH1/3H_2O + e \ . \tag{4}$$

For $E < 0.32$ V, a small mass decrease was corroborated to a hydrogen ejection leading to 70% of the coloration. For potential $E > 0.32$ V this process is superimposed to an OH^- injection with further coloration.

Electrochromic sol–gel $NiO–TiO_2$ layers have been recently developed and exhibit, when cycled in KOH electrolyte, a fast switching time (<10 s), a deep reversible brown coloration, a much better stability and a better adhesion to glass substrates than pure NiO layers [13,14].

The goal of the present investigation is to investigate the mass change of $NiO–TiO_2$ sol–gel layers, during cycling in 1 M KOH electrolyte using the EQCM technique in order to get a better understanding of the mechanisms of coloration and bleaching of such electrodes and to understand the role of the various phases on the stability and the degradation of these electrodes.

2. Experimental

An 0.5 M solution was prepared by dissolving 23.32 g of $Ni(CH_3COO)_2 \cdot 4H_2O$ in 150 ml ethanol at room temperature with continuous stirring for 7 h. Then 8.879 g of titanium *n*-propoxide were dissolved in 100 ml of ethanol and added to the Ni solution in a glove box filled with nitrogen (humidity RH $\leqslant 5\%$) to obtain sols with Ni/Ti molar concentration of 3/1. The sols were stirred at room temperature for 30 min, and finally filtered using a 0.2 μm Teflon filter.

Double $NiO–TiO_2$ layers with Ni:Ti ratio of 3:1 with a total thickness of about 160 nm thick were deposited on gold coated quartz crystal substrate (5 MHz AT-cut from Maxtek, Inc.) by the dip coating technique. The substrates were withdrawn from the precursor solution at a rate of 3 mm/s in ambient atmosphere (RH $< 60\%$). One side was covered to avoid the deposition of the layer on both sides of the crystal. The system was then sintered at 300 °C for 30 min in air.

The used electrochemical cell was a double wall glass flask connected to a water thermostat to control the temperature. The $NiO–TiO_2$ coated quartz crystal was used as working electrode, a platinum mesh as counter electrode and SCE as a reference electrode. 1 M KOH was used as electrolyte. The electrodes were fixed in three special holes in the rubber cap of the electrochemical cell. The EQCM measurements were made using a Maxtek, Inc microbalance connected to a multichannel potentiostat (model vmp2, Princeton Applied Research), in order to control the potential applied to the crystal. The frequency changes and the determination of the corresponding mass changes were obtained using the EQCM data logging software according to the Sauerbrey equation [9]:

$$\Delta f = -\left(\frac{2f_0^2}{A\sqrt{\mu\rho}}\right)\Delta m, \tag{5}$$

where Δf is the change in frequency (Hz), Δm the mass change (μg), f_0 is the resonant frequency of the used quartz crystal (5 MHz AT-cut), ρ is the density of the quartz (2.648 gcm^{-3}), A is the area of the electrode (1.37 cm^2) and μ is the quartz shear modulus (2.947 $\times 10^{11}$ $g\,s^{-2}\,cm^{-1}$). The minus sign indicates that the resonant frequency shifts to lower values by increasing the mass of the quartz crystal. The value in the parenthesis is the sensitivity factor of the crystal, $C_f = 56.6$ Hz $μg^{-1}\,cm^2$ and the above equation can be written in the simpler form

$$\Delta f = -C_f \Delta m. \tag{6}$$

All electrochemical parameters (i, Q) could be of course determined using this configuration. However, the quartz crystal electrode being opaque, no determination of the transmittance change could be measured and one had to rely on the results obtained using similar NiO–TiO$_2$ coatings deposited on a transparent FTO electrode (sheet resistance $R_\mu = 17\Omega_\mu$) [13,14].

3. Results and discussions

3.1. Electrochromism of NiO TiO$_2$ coating

This section gives a brief summary of the electrochromic behavior of NiO–TiO$_2$ layers deposited on FTO coated glass and cycled between -0.6 and $+0.6$ V vs. SCE in 1 M KOH electrolyte. Detailed results can be found in Refs. [13,14]. Typical CV cycles and transmittance change at 550 nm recorded simultaneously are shown in Fig. 1. The layers show a deep reversible brown coloration with a transmittance change measured at 550 nm between $T_{bleached} = 85\%$ and $T_{colored} = 25\%$ and a fast switching time (< 10 s). By extending the potential range to $+1$ V, the layers show even a darker brown color and a higher absorbance ($\Delta OD_{550} = 0.8$) with a high coloring efficiency.

The charge capacity Q_c has been calculated by integrating the cathodic waves in order to avoid any charge contribution of the oxygen evolution at positive potential (Fig. 2). The value, the number of cycles needed for charge stabilization and the stability of the layer are affected by the parameters of the layer processing (sintering temperature, number of layers, humidity, the scan rate) but especially by the thickness of the coating. An example is shown in Fig. 2 for a double layer 160 nm thick sintered at 300 °C. The cycling life is based on essentially two step processes consisting of an *activation period* and a complex *degradation period*.
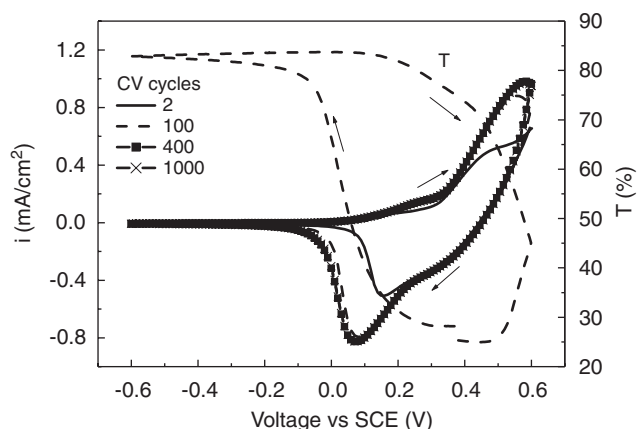

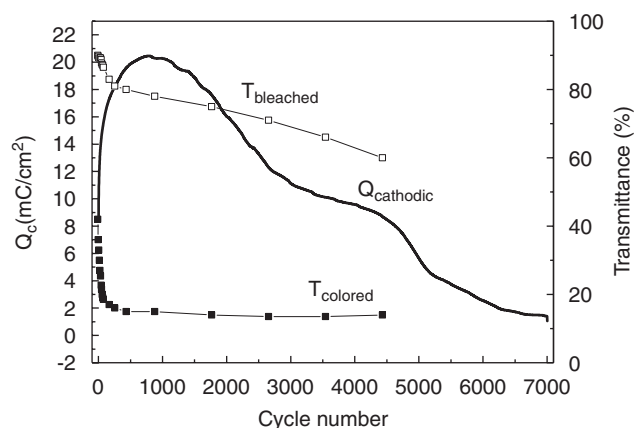
Fig. 2. Cathodic charge density and transmittance of the bleached and colored state measured at 550 nm vs. cycle number for a double (160 nm) NiO TiO$_2$ layer (Ni concentration of 75 mol %) deposited on K glass and heated at 300 °C. CV cycles: 0.6, 0.6 V vs. SCE, scan rate 10 mV/s in 1 M KOH (adapted from Ref. [13]).

In the first domain the charge density is rather low after the first cycle (5–8 mC/cm^2) and increases rapidly to reach a broad maximum 20.5 mC/cm^2 after 1000 cycles so that the coloration of the layer increases. This was interpreted to result from EC activity initiating in a thin interface layer (about 40–50 nm) that grows with cycling till reaching the full depth of the layer at the end of the activation period.

Practically simultaneously a slow degradation period takes place where a passive, irreversibly colored and fragile layer is built at the electrolyte/layer interface. This period is clearly observed after about 1000 cycles in which both the charge density and the optical density decrease continuously at a slow rate. An abrupt decrease of the charge even occurs around the 4500th cycles, its value becoming very small with drastic increase of the fragility of the layers.

In spite of the fact that no structural changes could be detected by XRD between uncycled and colored layers, rather large morphological changes have been observed by TEM. A fresh (uncycled) rasped thin layer shows many small round crystalline NiO grains with size of about 8 nm, i.e. about three times that of the crystallites, imbedded in an TiO$_2$ amorphous structure (Fig. 3a). A thin rasped layer measured in the colored state after 270 CV cycles (Fig. 3b) consists of many smaller NiO particles with size of about 3 nm i.e. the size of the NiO crystallites (2.5 nm), several of them aggregated in a filament shape together with some larger grains (size 10–13 nm) that have been interpreted as Ni(OH)$_2$ nanoparticles. This clearly indicates that the NiO grains have been disaggregated into their primary crystallites during cycling and that the layers have been hydrated. During cycling the layers become more amorphous and their structure consists of very small NiO crystallites linked probably with hydrogenated compounds and Ni(OH)$_2$ nanoparticles that cannot be identified by XRD.
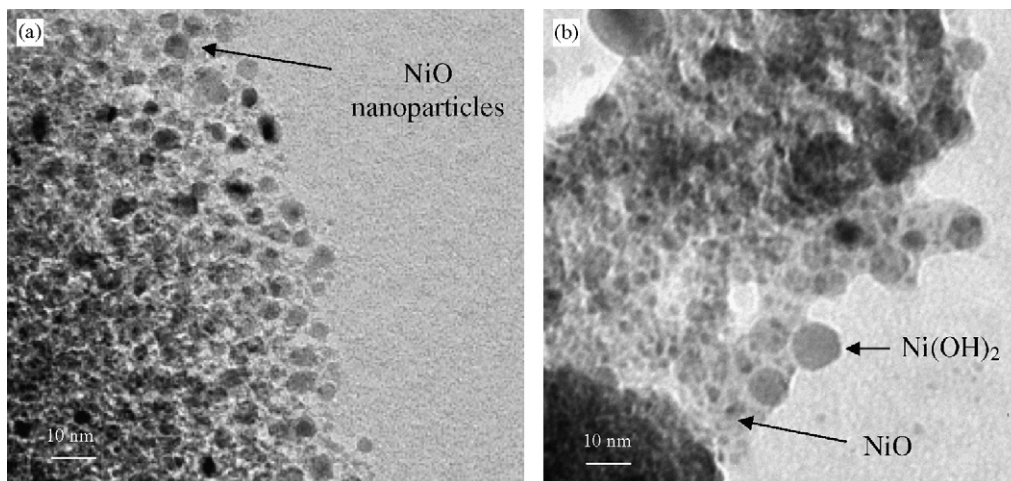

Fig. 1. Typical CV cycles up to 1000 cycles for a 160 nm thick double NiO TiO$_2$ layer (Ni concentration of 75 mol %) heated at 300 °C, potential range 0.6 to 0.6 V vs. SCE, scan rate 10 mV/s in 1 M KOH. The dotted line is the variation of the transmittance (T) measured during the 100th cycle at $\lambda = 550$ nm (from Refs. [13,14]).

Fig. 3. TEM pictures of NiO–TiO$_2$ rasped layers (Ni concentration of 75 mol %) deposited on K glass and sintered at 300 °C (a) fresh uncolored layer (b) colored layers after 250 cycles (from Refs. [13,14]).
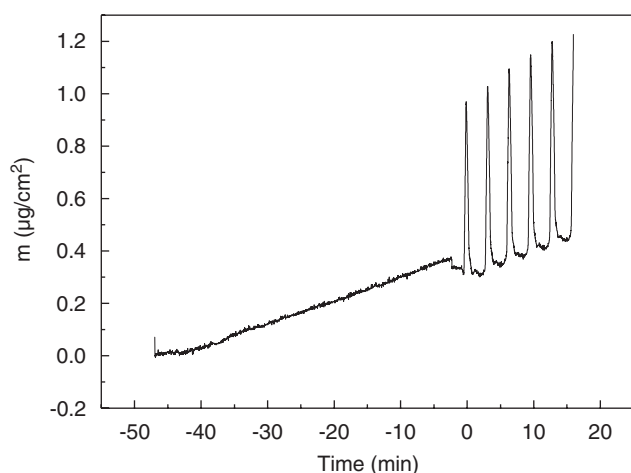

Fig. 4. Mass change at the open circuit potential (−0.11 V vs. SCE) during 47 min and then during the first five CV cycles.

Fig. 5. Lower figure: mass change during 650 CV cycles (−0.4 to +0.57 V vs. SCE, scan rate of 10 mV/s) for a NiO–TiO$_2$ double layer deposited on a quartz crystal, sintered at 300 °C, and tested in 1 M KOH. The value of the mass was set initially to zero at the beginning of the first cycle. Upper figure: cathodic and instant charge.

3.2. Envelope of the mass and charge change during cycling

The frequency of gold-coated quartz crystal was recorded before and after the layer deposition in order to estimate the mass of the layer. From the frequency shift, the mass of the deposited NiO–TiO$_2$ with Ni:Ti molar ratio of 3:1 was 5.8×10^{-9} g/cm^2. Assuming a density of 6.67 g/cm^3 for NiO and 4.25 g/cm^3 for TiO$_2$, the theoretical value of the mass of the layer will is $m = 9.66 \times 10^{-9}$ g/cm^2. This indicates that the layer has a rather high porosity of about 40%.

According to the recommendation of the balance manufacturer, the coated crystals were first left in the 1 M KOH electrolyte for 4 h before starting the measurements. Then the mass changes were recorded at the open circuit potential (−0.11 V) for 47 min. The system was afterwards cycled by applying a potential in the range −0.4 to +0.57 V vs. SCE at a scan rate of 10 mV/s. Fig. 4 shows the results of the mass change at the open circuit potential and during the first 5 CV cycles. Initially it slightly increases linearly at a rate of about 7 ng/cm^2/min, a value
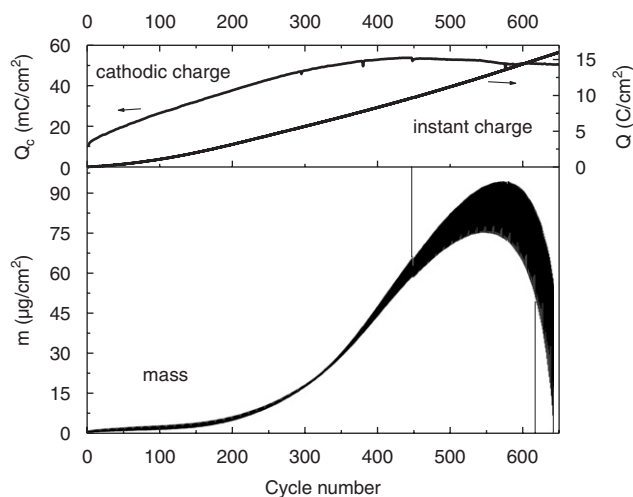
much smaller than the variation observed during the cycles. This is thought to originate from a slow change in the composition of the layer due to a wetting process occurring at the interface with possibly the growth of Ni(OH)$_2$. However, an electronic artifact cannot be excluded.

Fig. 5 shows the recorded evolution during 650 CV cycles of the mass, of the instant charge and of the cathodic charge integrated from the cathodic current. The values of the mass m and the instant charge Q have been set to zero at the beginning of the cycling.

The variation of the cathodic charge (Fig. 5) can be compared with that of Fig. 2 for a similar double layer deposited on FTO. The overall behavior up to 650 cycles is similar and certainly the results refer to what was called the *activation period*. It starts around the same value (9.2 mC/cm^2) then increases to a maximum value of 50 mC/cm^2 around the 450th cycle and finally slightly

decreases. The EC process of the layer deposited on gold-coated quartz substrate, as discussed in Section 3.1, should also initiate in a small thin layer at the interface electrolyte/layer, which grows during further cycling. However, the maximum value of the cathodic charge is higher than that of Fig. 2 and is reached after a smaller number of cycles. This is thought to be due to the more porous morphology of the layer ($P \approx 40\%$) that has been sintered on a metallic electrode instead of an FTO conducting oxide layer and that favors the charge exchange. The lower resistivity of the metallic electrode may also be responsible as the shape of the CV voltammograms is slightly different (Fig. 6). In particular the O_2 evolution is clearly seen at a lower potential ($+0.5$ V instead of $+0.57$ V). Unfortunately, as discussed below it was not possible to record the parameters during the degradation period (>1000 cycles).

The spectrum of the recorded instant charge (Fig. 4) shows a continuous increase with cycling. If the system was only involving fully reversible intercalation/deintercalation processes the records should have been a straight horizontal line close to $Q = 0$. It is not the case and as found for layers deposited on FTO [13,14], part of the recorded charge is used for side reactions that do not involve a mass exchange and coloring/bleaching effect. This is the case e.g. of O_2 and H_2 evolution that occurs in the electrolyte. This also explains the change observed in the values of the current density.

The shape of the mass spectrum (lower part of Fig. 5) is rather complex and changes continuously by cycling. The mass of the layer increases after each cycle rather slowly up to 1/3 of the *activation period* (i.e. up to about 150 cycles) and then starts to increase particularly strongly after about 250 cycles. It passes through a high maximum near the 570th cycle with high amplitude variation within each cycle and finally decreases fast even though the values of the cathodic charge decrease only slightly. Finally, a complete breakdown occurs around the 650th CV cycle from which
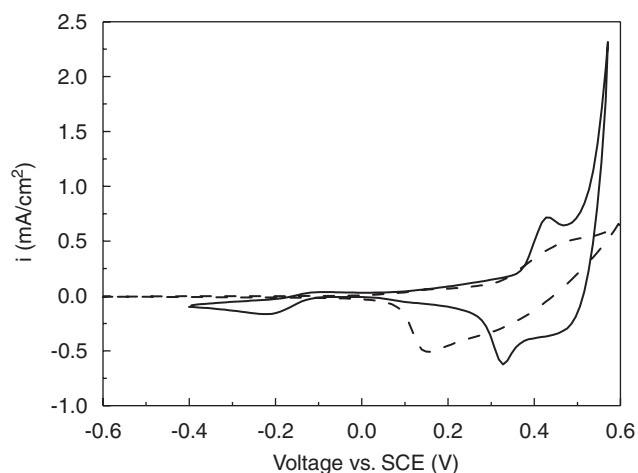
it was not possible to record any mass variation. This last behavior was observed with all tested layers and seems to be due to an unknown technical problem.

Two features are particularly interesting:

The first one is clearly seen on Fig. 5: the amplitude variation of the mass during each cycle, reflected by the width of the curve, is strongly dependent on the cycle number. It slowly increases from the first cycle up to about the 150th cycle, remains almost stable up to 200th cycle and then decreases to practically zero around the 330th cycle. Then it strongly increases to reach values as high as 40–50 $\mu g/cm^2$/cycle around the 600th cycle.

The second feature is observed by a closer look at these variations, which shows that the kinetics of the mass change during each cycle is also continuously changing. The study was divided in several typical regions described in the next sections.

3.3. From the first to the 150th CV cycle

This period corresponds to about one third of the so-called *activation period*. Fig. 7a shows the mass and charge changes during the first 5 CV cycles. Although the measurements have been initiated at the open circuit
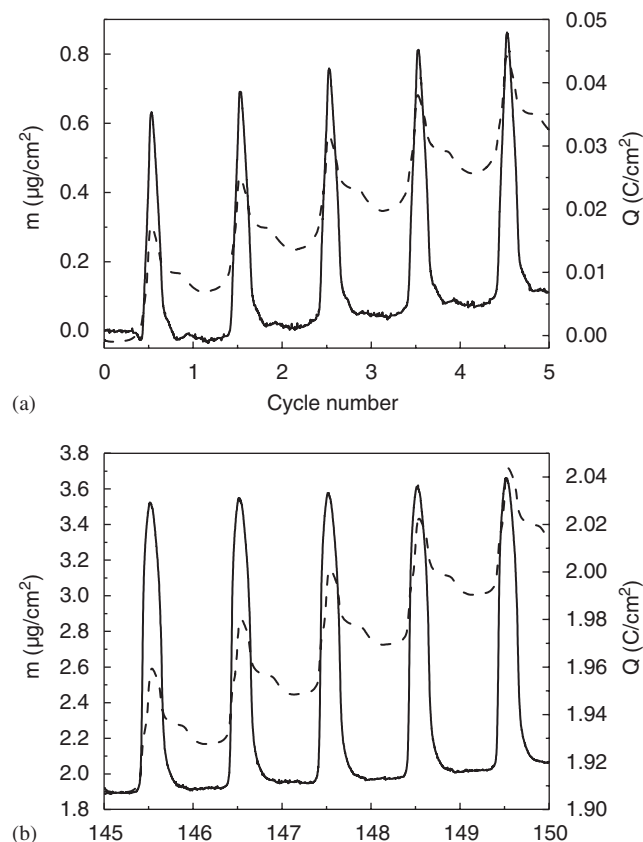

(a)

(b)

Fig. 7. Top: mass ( ) and charge ( ) changes during the first five CV cycles (0.4, $+0.57$ V, scan rate 10 mV/s) for a NiO TiO₂ double layer deposited on quartz crystal substrate and tested in 1 M KOH. Lower: same for the 145th 150th cycles. The origin of each abscissa corresponds to a potential value of 0.4 V vs. SCE.

Fig. 6. Second CV voltammograms in 1 M KOH of NiO TiO₂ double layer deposited on FTO coated glass ( ) and gold coated quartz ( ) with a withdrawal speed of 3 mm/s and sintered at 300 °C.

potential (-0.11 V), for an easier discussion, the results are presented initiating at the most negative potential (-0.4 V) corresponding to the bleached state of the layer. The potential scan is performed in the direction of positive potential up to $+0.57$ V, and then back to the negative potential. The initial ordinate values for m and Q have been reset to zero. The lower figure shows the results recorded between the 145th and 150th CV cycle.

The overall behavior of the mass and the charge in each cycle is similar. They increase in the anodic range and decrease in the cathodic one so that the physical processes are basically the same up to 150 cycles. However, one observes that:

I. The change of the mass is $0.65\,\mu g/cm^2$ during the first cycle and increases to a value of $1.6\,\mu g/cm^2$ during the 150th cycle (value then stable up to the 200th cycle).
II. The mass exchange is not fully reversible within each cycle so that the mass of the layer increases continuously and linearly during cycling at a rate of about $30.4\,ng/cm^2/cycle$. Taking into account the time required to perform the measurement (194 s/cycle) this value corresponds to $9.4\,ng/cm^2/min$ i.e. a value quite close to that observed at the open circuit ($7.0\,ng/cm^2/min$).
III. The peak height of the charge is $0.017\,C/cm^2$ during the first cycle and increases to $2.042\,C/cm^2$ during the 150th cycle.
IV. The charge is also not reversible and increases continuously but not linearly, initially at a rate of $6.7\,mC/cm^2/cycle$ to reach a value of $20\,mC/cm^2/cycle$ during the 150th cycle.

In order to better understand these observations the voltamassogram and voltammogram of the second cycle are shown on an enlarged scale in Fig. 8 and in a mass vs. charge representation in Fig. 9.
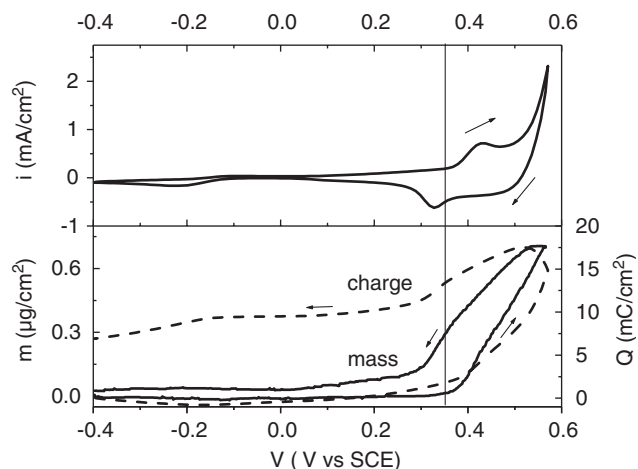

Fig. 8. Voltammogram and voltmassogram of NiO TiO$_2$ double layer deposited on gold coated quartz crystal recorded during the second CV cycle (-0.4 to $+0.57$ V, scan rate $10\,mV/s$).
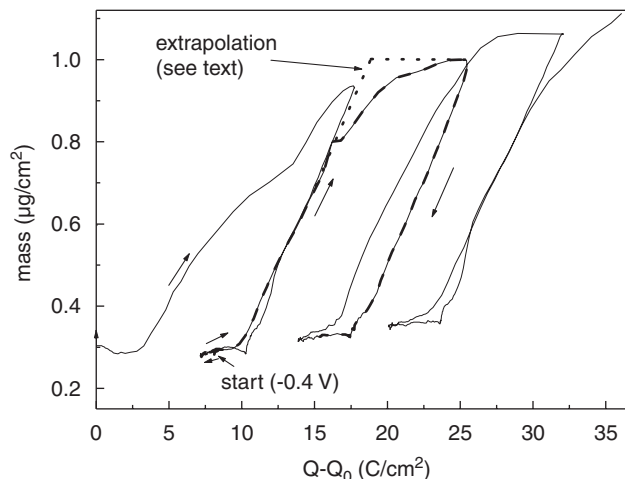

Fig. 9. Mass change against charge change of a NiO TiO$_2$ double layer deposited on gold coated quartz crystal during the first three CV cycles (-0.4 to $+0.57$ V, scan rate $10\,mV/s$). The second cycle is highlighted.

3.3.1. Second cycle

The mass increases in the anodic scan and decreases in the cathodic one and the mass of the layer slightly increases at the end of the cycle by about $0.03\,\mu g/cm^2$. In the anodic scan, no mass change and very little charge increase are observed in the potential range -0.4 to $+0.35$ V vs. SCE. The mass and charge start to increase at 0.35 V together with the current density. A well-defined anodic peak then occurs with a maximum at $+0.43$ V. It is correlated with the layer coloration (see Fig. 1) and at the peak maximum the transmittance has decreased by about 50%. The mass passes by a maximum before the end of the anodic range but the charge, as it should be, passes by a maximum at the end of the anodic scan when $i = 0$. A large current density peak related to an O$_2$ evolution is superimposed at the end of the anodic scan. In the cathodic region, a minimum of the current density is observed at around 0.32 V corresponding to the layer bleaching (see Fig. 1) as well as a very low intensity broad cathodic peak around -0.22 V. The first peak is accompanied by a decrease of the mass and the charge and the second one by a decrease of the charge and a very slight increase of the mass. The total charge does not return to the initial value ($Q-Q_0 = 6.7\,mC/cm^2$) and this value corresponds probably to the charge used during the oxygen evolution. However, the mass almost returns to its initial value so that the total mass of the layer only increases by about $0.03\,\mu g/cm^2$. It is worth to mention at this point that this second CV voltammogram, except for the features observed around -0.22 V, presents the same features of that measured for a similar layer deposited on a FTO coated glass substrate (see Figs. 1 and 6).

Another representation is helpful for the discussion of the results. Fig. 9 shows a plot of the mass against the charge for the first three cycles. Considering again the second cycle, one clearly sees, starting at -0.4 V vs. SCE, a small decrease then a slight increase of the charge without any meaningful change in the mass. Then the

mass increases first linearly with the charge with a slope of $80\,\mu g/C$ and then the slope decreases to zero when the mass reaches a maximum value. When the charge decreases, the mass decreases proportionally with the same slope ($80\,\mu g/C$) down to a point where there is no mass variation but still a decrease of the charge.

The change of the slope (to almost zero value) is rather easy to understand as it occurs during the O_2 evolution confirming that part of the recorded charge is used for a reaction that does not involve a mass change. It is therefore expected that the mass continues to increase linearly up to a plateau as shown by the dotted line in Fig. 8 (extrapolation).

3.3.2. 145th cycle

Fig. 10 shows the voltammogram, voltamassogram and the variation of the charge measured during the 145th cycle.

The overall behavior is similar to that shown for the second cycle (Fig. 8). However, several important differences can be observed:

I. The height of the current density peak related to the electrochromism in both the anodic range (at $V = 0.43\,V$) and in the cathodic range (at $V = 0.32\,V$) are much higher. The current peak is also better separated from the current related to the O_2 evolution.

II. As before, the change of the mass is strictly zero up to $+0.35\,V$ but the peak value is much higher ($1.6\,\mu g/cm^2$ vs. $0.65\,\mu g/cm^2$) and also occurs before the end of the anodic cycle. The potential at which the mass increases is slightly shifted to more positive potential.

III. The charge exchanged in the anodic range is also much higher ($53\,mC/cm^2$ vs. $17\,mC/cm^2$). The net charge is also higher ($2.04\,C/cm^2$ vs. $0.017\,C/cm^2$) and as before is not reversible.

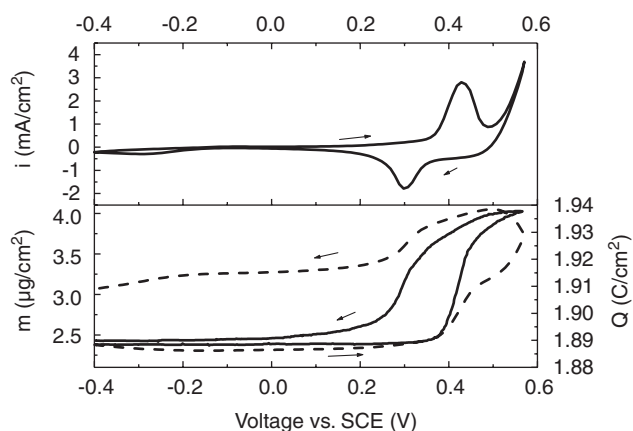IV. The small cathodic peak around $-0.22\,V$ also increases.

Fig. 10. Voltammogram and voltmassogram of a NiO TiO$_2$ double layer deposited on gold coated quartz crystal during the 145th CV cycle (0.4 to $+0.57\,V$, scan rate $10\,mV/s$).
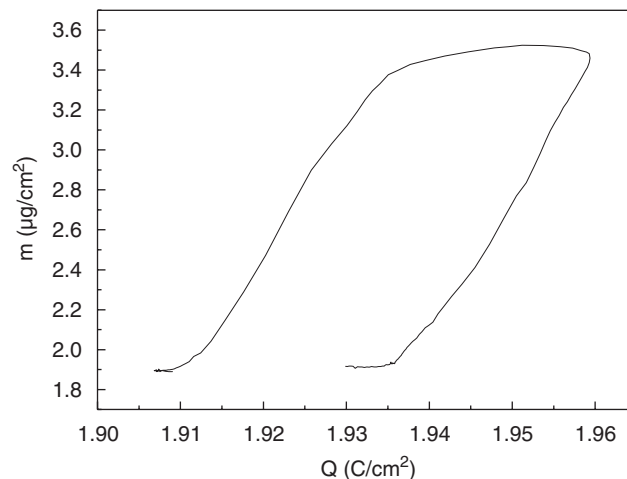

Fig. 11. Mass change against charge change of a NiO TiO$_2$ double layer deposited on gold coated quartz crystal during the 145th CV cycle (0.4 to $+0.57\,V$ scan rate $10\,mV/s$).

Finally, Fig. 11 shows the plot of the mass versus charge for the 145th cycle. The shape and the behavior are quite similar to those shown for the second cycle and both linear variations have exactly the same slope as before, $80\,\mu g/C$, but the maximum before the end of the anodic cycle is higher ($1.6\,\mu g/cm^2$ vs. $0.65\,\mu g/cm^2$). At the end of the anodic range the slope decreases to zero for the same reason given above to explain the behavior of the second cycle (O_2 evolution).

3.3.3. Model

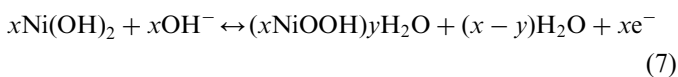During the activation period up to 150th cycle two main features are observed:

a) A variation of the charge without variation of the mass in the anodic range from -0.4 to $0.35\,V$ and in the cathodic range from 0 to $-0.4\,V$ vs. SCE.

This feature is different from that observed by Bange et al. [12] for NiO layers produced by *e-beam evaporation* where a small decrease of the mass was observed during the first part of the anodic cycle explained as an evidence for a hydrogen ion ejection. For the sol–gel layers there is no mass evolution in this range. Therefore, the process, responsible of the small cathodic wave around $-0.22\,V$ should only involve reaction(s) with electrons. The wave is however not seen in the voltammograms of layers deposited on FTO (see Fig. 1) whatever is the potential range. Moreover, as seen later, this wave becomes much more pronounced as cycling proceeds. The discussion of its origin will be presented therefore later.
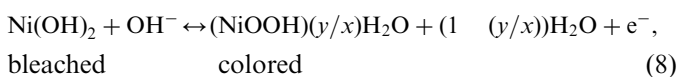
b) A linear increase of the mass in the anodic range and a linear decrease of the mass in the cathodic range with the same slope ($80\,\mu g/C$).

This feature is without any doubt related to an almost fully reversible exchange of OH$^-$ groups that involves a change of the oxidation state of Ni from 2^+ to 3^+ and vice versa at a lattice site leading to the coloration and bleaching processes, respectively.

The increase of the current density, charge and mass with cycling are compatible with the ideas proposed in Section 3.1 and [14] that, in this activation period, only a thin layer located at the interface electrolyte/layer is active and that the thickness of this layer increases by cycling. Without knowing with precision the complex surroundings of the NiO nanparticles, where the presence of $Ni(OH)_2$ (not observed by X-ray but only by TEM) and H_2O too is expected either because of the low sintering temperature and/or by the wetting of the layer in the electrolyte, a precise model cannot be proposed. One possible equation to describe the results for $E > 0.35\,V$ is

$$x Ni(OH)_2 + x OH^- \leftrightarrow (x NiOOH) y H_2O + (x - y) H_2O + x e^- \tag{7}$$

and dividing by x

$$Ni(OH)_2 + OH^- \leftrightarrow (NiOOH)(y/x) H_2O + (1 \quad (y/x)) H_2O + e^-,$$
bleached $\qquad$ colored $\hfill(8)$

with $0 \leqslant y \leqslant x$

The x value is an arbitrary number greater than zero that describes the bonding of x hydroxyl ions per $Ni(OH)_2$ during the coloration of the film and the equation suggests the formation of NiOOH and y/x lattice water bonded to NiOOH due to the incorporation of OH^- and the transfer of $(1-y/x)$ water into the electrolyte.

According to this equation the change in mass of the sol–gel layer during the second cycle will be

$$M_w = (y/x) M_{H_2O} - M_H, \tag{9}$$

$$M_w = (y/x)(18) - 1. \tag{10}$$
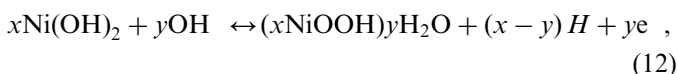
Using the equation relating mass and charge changes
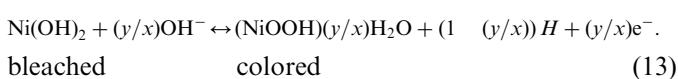
$$\Delta m = (\Delta Q/F) M_w, \tag{11}$$

where Δm is the change of the mass ($\mu g/cm^2$), ΔQ is the variation of the charge (C/cm^2), F is the Faraday constant ($96485\,C/cm^2$) and M_w is an apparent molar mass of the involved species, and using the obtained value of the slope $\Delta m/\Delta Q = 80\,\mu g/C$ it is found that $M_w = 7.7\,g/mol$.

Using this value in Eq. (10), the value of y/x is $8.7/18 \approx 0.5$.

Another possible but slightly different reaction that gives the same $y/x \approx 0.5$ value is

$$x Ni(OH)_2 + y OH \leftrightarrow (x NiOOH) y H_2O + (x - y) H + y e \ , \tag{12}$$

with $0 \leqslant y \leqslant x$ and dividing by x

$$Ni(OH)_2 + (y/x) OH^- \leftrightarrow (NiOOH)(y/x) H_2O + (1 \quad (y/x)) H + (y/x) e^-.$$
bleached $\qquad$ colored $\hfill(13)$

This equation is similar to that proposed by Bange et al. [12] except that in our case about 0.5 hydrogen ion per $Ni(OH)_2$ will be evolved *only* during the coloration process

i.e. for $V > 0.35\,V$ and not during the earlier part of the anodic cycle.

Both proposed reactions (8) and (13) may not be 100% reversible so that the layer becomes richer in hydrated NiOOH leading to a slight but continuous increase of the permanent coloration.

These two proposals involve only reactions between $Ni(OH)_2$ and OH^-. However, it was observed during the first 150 cycles that the total mass of the layer increases after each cycle by $0.034\,\mu g/cm^2$ and that the mass exchange during each cycle was initially $0.65\,\mu g/cm^2$ but reached a value of $1.6\,\mu g/cm^2$ after 150 cycles. Also the charge exchange during each cycle increases from $17\,mC/cm^2$ at the second cycle to $53\,mC/cm^2$ after 150 cycles leading to an increase of the coloration of the layer. Therefore, the amount of $Ni(OH)_2$ available for these reactions also has to increase. This may be related to the following irreversible reaction:

$$NiO + 2H_2O \leftrightarrow Ni(OH)_2 + (1 - z) NiO.$$
nonactive $\qquad$ ECactive $\hfill(14)$
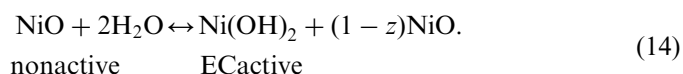
If the continuous increase of the mass after each cycle ($0.034\,\mu g/cm^2$) is due to this reaction, this will involve a value of $z = (3.4 \times 10^{-8}\,g/cm^2)/(18\,g/mol) = 1.8 \times 10^{-9}\,mol/cm^2$ of water, taken either from the electrolyte or from the layer. The NiO particles being rather dense, the reaction should occur on the surface of the particles. This leads to a continuous decrease of the amount of the NiO in the layer as observed by XRD and TEM (Fig. 3) [14].

It is not possible to give better explanations without a better knowledge of the composition of the layer. This model nevertheless allows to explain why the mass of the layer increases, why the layer becomes fragile (higher hydration) and also why a higher sintering temperature ($T > 400\,°C$) was not suitable for the electrochromic properties (less hydration) [14].

Although the proposed equation is somewhat different from that of Bange et al. [12], the latter conclusions are in agreement with it. One can therefore propose the following compositions for the bleached and colored layers:

$$\text{bleached state} \quad NiO + x(NiOH)_2 + TiO_2, \tag{15}$$

$$\text{colored state} \quad NiO + (x NiOOH) y H_2O + TiO_2, \tag{16}$$

where the values of x and y change continuously during cycling.

3.3.4. From the 150th cycle

The voltammograms and voltamassograms of the 200th, 300th, 330th and 400th cycles are shown in Fig. 12. The value of the mass at $V = -0.4\,V$ vs. SCE has been reset to zero for all records for better comparison. They were 4.76, 17.64, 24.42 and $47.4\,\mu g/cm^2$, respectively. Also, for a better comparison, the same scale of the ordinates has been used for each cycle.

Fig. 13. Voltammogram and voltmassogram for a NiO TiO$_2$ double layer deposited on gold coated quartz crystal during the 330th CV cycle (0.4, 0.57 V, scan rate 10 mV/s).
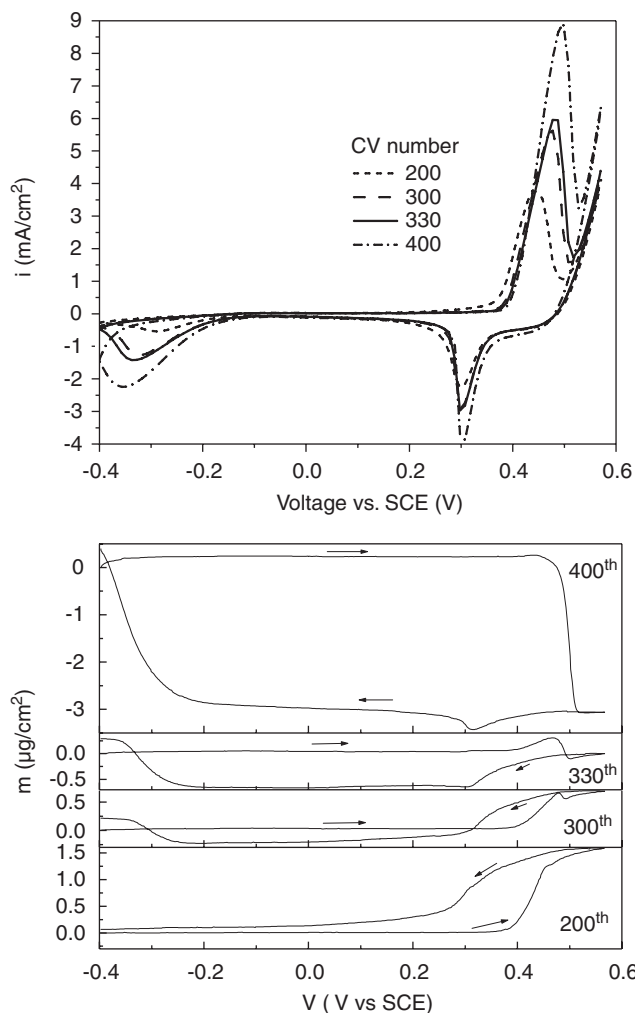
Fig. 12. CV voltammograms and voltamassograms of the 200, 300, 330 and 400th CV cycles of NiO TiO$_2$ double layer deposited on gold coated quartz crystal, sintered at 300 °C and tested in 1 M KOH in the potential range 0.4 to 0.57 V scan rate 10 mV/s. For better comparison the ordinate scales of the mass are the same in all graphs.

The electrochromic anodic peak in the range of 0.43 V vs. SCE grows continuously so that the ratio of the intensity of this peak to that of the oxygen evolution increases. The anodic peak position is also slightly shifted to higher positive potential values by cycling. The first cathodic peak around +0.3 V vs. SCE increases also but practically does not shift by cycling. The second one at the end of the cathodic scan at −0.3 V vs. SCE drastically increases by cycling and shifts to more negative potential values.

The shape of the voltamassogram during the 200th CV cycle (lower part of Fig. 12) is similar to that of the 150th cycle (see Fig. 10) and the mass increase occurs during the anodic scan at a voltage corresponding to the anodic current peak. There are then however drastic changes between the 200th cycle and the 400th cycle.

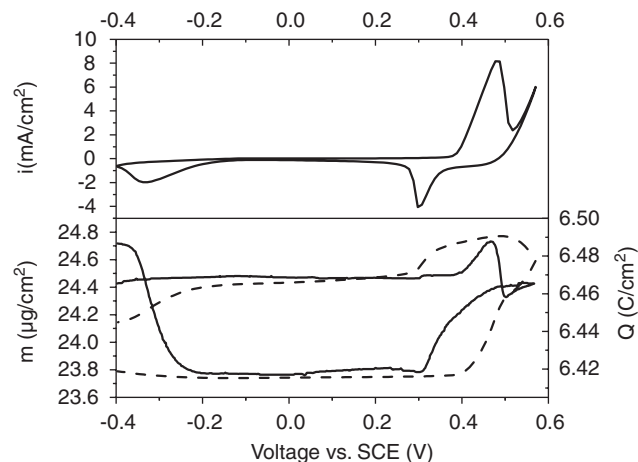As before no mass change is observed in the first part of the anodic cycle but the potential range slightly increases to more positive values from +0.4 V at the 200th cycle to +0.47 V at the 400th cycle.

The behavior at the end of the anodic cycle becomes rather complicated. The mass increase is continuously reduced but it can still be observed up to about the 377th cycle. It is substituted by a mass decrease around 0.48 V vs. SCE that can be observed already at the 300th cycle and that occurs in a very small potential range (0.48–0.52 V vs. SCE). At this stage the absolute value of the mass change passes by a minimum (0.9 μg/cm^2). Its value then drastically increases with cycling to reach a value of 4 μg/cm^2 at the 400th cycle. This can be clearly observed by the width of the mass records in Fig. 5.

At the end of the cathodic cycle a mass increase is now observed initiating at around −0.22 V vs. SCE linked clearly to the increase of the height of the second cathodic current peak. Its value grows with cycling to reach about 4 μg/cm^2 at the 400th cycle. It should be remembered that this cathodic peak was not observed by studying NiO–TiO$_2$ layers deposited on FTO conducting layer (see Fig. 1).

The 330th cycle was found as a good example for studying this transition period in more detailed manner (Fig. 13).

In the anodic range, both the charge and the mass of the layer remain constant up to +0.4 V where a sharp increase in the charge and mass are noticed corresponding to the anodic electrochromic peak. The mass starts to decrease sharply at 0.45 V before increasing again.

By reversing the potential scan, a clear decrease of the charge and the mass occurs around +0.3 V corresponding to the first cathodic peak. A slight decrease of both the mass and charge is seen down to −0.25 V where a sharp decrease of the charge starts with a large mass increase corresponding to the cathodic peak centred at −0.3 V.

It is difficult at this stage to know exactly what is occurring during this transition period. Nevertheless, Figs. 14 and 15 show a plot of the mass change vs. charge change for the 330th and 400th cycle, respectively. In the
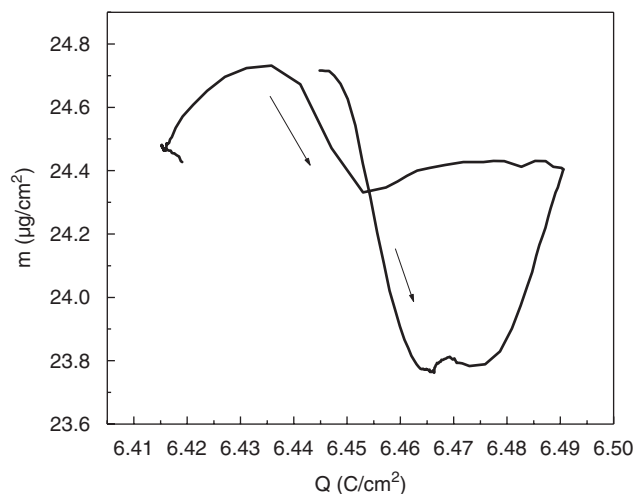
Fig. 14. Mass change against charge change of a NiO TiO$_2$ double layer deposited on gold coated quartz crystal during the 330th CV cycle (0.4 to $+0.57$ V, scan rate 10 mV/s).

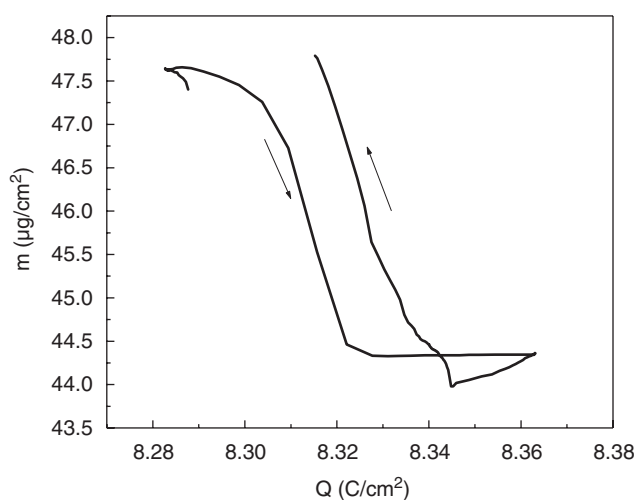Fig. 15. Mass change against charge change of a NiO TiO$_2$ double layer deposited on gold coated quartz crystal during the 400th CV cycle (0.4 to $+0.57$ V scan rate 10 mV/s).

latter graph the decrease and increase of the mass have a similar behavior with a higher slope of about 181 μg/C.

Finally, Fig. 16 shows the voltammogram and voltamassogram for some of the last cycles (450th, 500th, 590th, 650th cycles). As before the mass values have been set to 0 at -0.4 V.

The shape of the CV voltammograms remains essentially constant. Compared to the 400th cycle the intensity of the anodic current peak around 0.5 V has slightly decreased from 9 to 6.5 mA/cm^2 and has slightly shifted to higher positive potentials. The first cathodic peak around 0.3 V vs. SCE and the one at the end of the cathodic scan at -0.35 V vs. SCE both have also decreased.

The corresponding mass changes are shown in the lower part of Fig. 16. They are compatible with the voltammo-
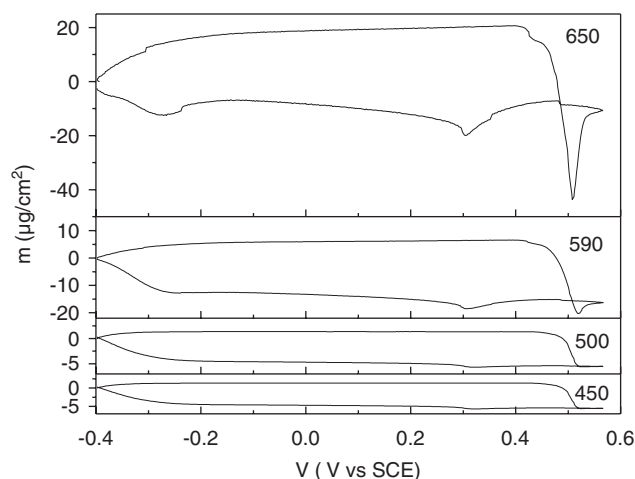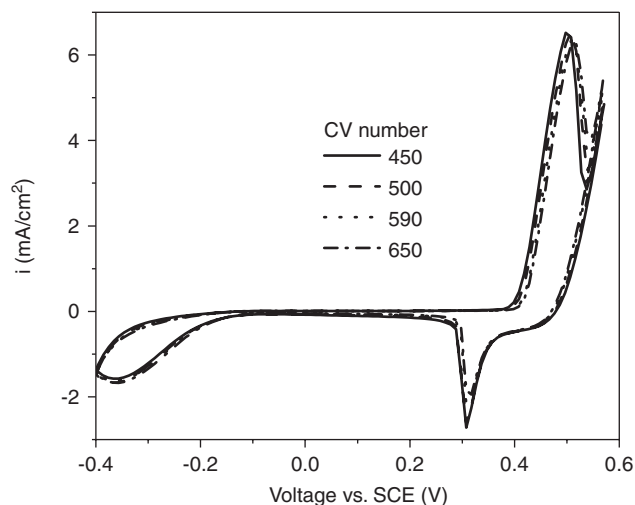

Fig. 16. CV voltammograms and voltamassograms of the 450, 500, 590 and 650th CV cycles of NiO TiO$_2$ double layer deposited on gold coated quartz crystal, sintered at 300 °C and tested in KOH in the potential range 0.4 to 0.57 V scan rate 10 mV/s. The mass values have been set reset to zero at 0.4 V and the scales are the same in all four graphs.

grams. The shape of the spectra up to the 550th cycle is similar to that of the 400th cycle (Fig. 12). One observes however a very large increase of the mass change from 4 μg/cm^2 at the 400th cycle up to 63 μg/cm^2 at 650th cycle. Also, during the last cycles a mass increase becomes again superimposed at the end of the anodic cycle. As the cathodic peak at the end of the cathodic scan shifts to more negative potentials, the corresponding mass increase shifts in the same direction so that it is only completed in the anodic scan.

3.4. Model

The results obtained till the 150th cycle have been correlated to the exchange of OH$^-$ ions during the CV cycles that react with Ni(OH)$_2$ to produce hydrated NiOOH (responsible for the coloration of the layer), as well as intercalated water molecules that react with NiO to increase the amount of Ni(OH)$_2$ in the layer to explain the

increase of ΔOD and the decrease of the size of the NiO nanoparticles by cycling. These changes in the layer composition are clearly associated by an increase of the porosity and fragility. From the 330th cycle one observes a drastic change of the mass spectra that can only be explained by a partly irreversible exchange of positive ions and these can only be K^+ or hydrated $K(H_2O)_n^+$ ions, the primary hydration number of K being 4 [15]. A similar behavior has been recently observed by Sun [16] for CeO_2–TiO_2 sol–gel counter electrode layer tested in wet $LiClO_4$-PC electrolyte. The high weight of the ions explains why the ratio mass/charge during the 400th cycle is higher ($181\,\mu g/C$ vs. $80\,\mu g/C$) and why the total mass increases after each cycle drastically up to 570 cycles. The layer morphology and structure become therefore very loose up to a point that the layer breaks down and is dissolved in the electrolyte (observed at the 650th cycle).

4. Conclusion

The coloration and bleaching mechanisms of NiO–TiO_2 sol–gel electrochromic layers sintered at $300\,°C$ have been studied in KOH electrolyte during 650 CV cycles using a quartz crystal microbalance (QCM) in the potential range -0.4 to $+0.57$ V vs. SCE. Models have been suggested and discussed. The fresh layers consist of NiO nanoparticles imbedded in an amorphous structure of TiO_2. The increase of the current density, charge and mass during the first 250 cycles are compatible with the ideas proposed in Refs. [13,14] that, in the activation period, only a thin layer located at the interface electrolyte/layer is active and that the thickness of this layer increases by cycling. Without knowing with precision the complex surroundings of the NiO nanoparticles, where the presence of $Ni(OH)_2$ and H_2O is expected because of the low sintering temperature and by the wetting of the layer in the electrolyte, the results have been interpreted assuming that OH^- ions are exchanged leading to an irreversible increase of both the mass and charge exchanged during each cycle. This causes an increase of the amount of $Ni(OH)_2$ at the expense of the NiO nanoparticles and a simultaneous reversible bonding of hydroxyl ions to $Ni(OH)_2$ with formation of hydrated NiOOH giving rise to the coloration of the film, the equation suggesting also the formation of lattice water. This allowed to understand the increase of the coloration of the layer and the change of its morphology as observed by the TEM measurement.

The gradual change of the morphology leads also to a more open and mechanically fragile structure so that by further cycling unusual large increase of the mass of the layer during each cycle has been observed after the 330 cycles. This was interpreted as due to the incorporation of K^+ ions or $K(H_2O)_n^+$ that degrade the layers and leads to a complete break down observed after 650 cycles.

Acknowledgements

References

[1] P.R. Bueno, T.R.C. Faria, L.O.S. Bulhõ Es, Solid State Ionics 176 (2005) 1175.
[2] A. Surca, B. Orel, J. Sol–Gel Sci. Technol. 8 (1997) 743.
[3] M.C.A. Fantini, SPIE Proc. 1536 (1991) 81.
[4] J.-Y. Park, K.-S. Ahn, Y.-C. Nah, H.-S. Shim, J. Sol–Gel Sci. Technol. 31 (2004) 323.
[5] A. Azens, L. Kullman, G. Vaivars, H. Nordborg, C.G. Granqvist, Solid State Ionics 113–115 (1998) 449.
[6] I. Bouessay, A. Rougier, P. Poizot, J. Moscovici, A. Michalowicz, J.-M. Tarascon, Electrochim. Acta 50 (2005) 3737.
[7] M.K. Carpenter, R.S. Conell, D.A. Corrigan, Solar Energy Mater. 16 (1987) 333.
[8] J. Scarminio, W. Estrada, A. Andersson, A. Gorenstein, F. Decker, J. Electrochem. Soc. 139 (1992) 1236.
[9] P. Bernard, C. Gabrielli, M. Keddam, H. Takenouti, Electrochem. Acta 36 (1991) 743.
[10] T. Ohligschläger, G. Schwitzgebel, Phys. Chem. Chem. Phys. 3 (2001) 5290.
[11] S.I. Cordoba-Torresi, C. Gabrielli, A. Hugot-Le Goff, R. Torresi, J. Electroanalytical Chem. 138 (1991).
[12] A. Nemetz, A. Temmink, K. Bange, S.C. De Torresi, C. Gabrielli, R. Torresi, A. Hugot-Le Goff, Solar Energy Mater. Solar Cells 25 (1992) 93.
[13] A. Al-Kahlout, Ph. D. Thesis, University of Saarland and Leibniz-Institut für Neue Materialien- (INM) and University of Saarland, 2006.
[14] A. Al-Kahlout, S. Heusing, M.A. Aegerter, J. Sol–Gel Sci. Technol. 39 (2006) 195.
[15] F.A. Cotton, G. Wilkinson, The Group IA (1) Elements Li, Na, Rb, Cs, Fr, Wiley, USA, 1988 (Chapter 4).
[16] D. Sun, Ph.D. Thesis, Leibniz Institute for New Material-INM and University of Saarland, Saarbruecken, 2005.